ACS APPLIED MATERIALS & INTERFACES

Research Article

www.acsami.org

Synergistic Anticancer Activity of Fluorescent Copper Nanoclusters and Cisplatin Delivered through a Hydrogel Nanocarrier

Rama Ghosh,[†] Upashi Goswami,[‡] Siddhartha Sankar Ghosh,[‡,§] Anumita Paul,*[,†] and Arun Chattopadhyay*[,†,‡]

[†]Department of Chemistry, [‡]Centre for Nanotechnology, and [§]Department of Biotechnology, Indian Institute of Technology Guwahati, Guwahati-781039, Assam, India

Supporting Information

ABSTRACT: Highly fluorescent red copper nanoclusters (Cu NCs) were synthesized in aqueous medium in the presence of dihydrolipoic acid and poly(vinylpyrrolidone) (PVP). The Cu NCs, in solid form, were stable, retained their optical properties for a month, and could be redispersed for use when required. The NCs in aqueous medium exhibited pH-tunable reversible optical properties. The PVP stabilized NCs, when converted into hydrogel by cross-linking with poly(vinyl alcohol), delivered anticancer drug to cervical cancer (HeLa) cells, thereby inducing apoptotic cell death. The red emission properties of the Cu NCs in the hydrogel were used for optical imaging as well as for flow cytometric probe of cellular uptake. Cell viability assay, Caspase3 assay, and cell cycle analyses demonstrated that the Cu NCs present in the hydrogel composite exhibited synergy of action, along with the drug, cisplatin, against HeLa cells.

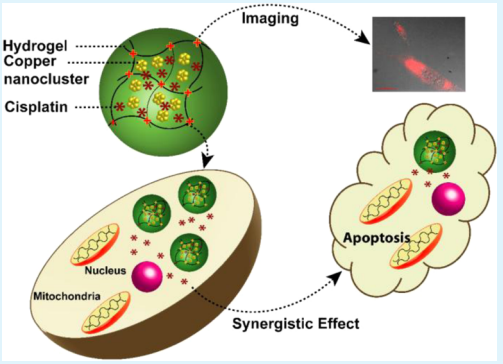

KEYWORDS: *copper nanoclusters, biolabeling, cisplatin, hydrogel, drug delivery*

INTRODUCTION

Metal nanoclusters (NC) bridge the materials gap between atom and nanoparticle (NP). The inherent quantum behavior of the NCs makes them a promising material endowed with size, tunable optical, and the other physical properties. Smaller size, reasonable chemical stability, excellent photostability, low cytotoxicity, and high luminescence quantum yield (QY) collectively provide a better prospect for using the noble metal NCs (especially Au NCs) in biological applications, instead of semiconductor quantum dots, which are generally cytotoxic. Recent surge of reports on their use for sensing,[1−3] biolabeling, bioimaging,[4−7] and chemical catalysis[8−10] is a testimony to their growing importance.

An important parameter that decides the utility of the NCs is their stability in liquid media, especially in the milieu of chemically and biochemically active moieties. This is where the development of new methods play important role in generating physically and environmentally responsive NCs. Among the noble metals, NCs of Au and Ag have been synthesized using templates such as polymer,[11,12] DNA,[13,14] protein,[15−17] and thiol-containing smaller molecular entities.[18] The inherent chemical stability of Au and Ag favors the synthesis of their NCs with comparative ease as opposed to those of Cu. The case of Cu NC is particularly difficult because of its instability even in mildly oxidizing condition. However, recent experiments from our laboratory[19] and others suggest that it is possible to synthesize stable Cu NCs. For example, Cu NCs have been synthesized using 2-mercapto-5-*n*-propylpyrimidine[20] and D-penicillamine[21] as protecting ligands. Also, etching of Cu NPs along with the use of glutathione (GSH) as a stabilizing ligand resulted into monodispersed fluorescent Cu NCs.[22] On the other hand, Cu NCs synthesized in the presence of DNA have been used to identify single nucleotide polymorphism.[23] Further, blue and red-emitting Cu NCs, synthesized in the presence of protein such as lysozyme[19] and BSA,[24] have been used in cell labeling applications. As mentioned above, while there are a few methods available for the synthesis of Cu NCs, there are still demands for Cu NCs with high stability and having application-specific stabilizing molecules or structures. For example, there is a need for obtaining stable red-emitting Cu NCs. In addition, if the NCs could be stabilized in the form of solid composites it would be better for storage, transport, and further use. That copper is an important and essential trace element in human, that there are sequestering agents for copper,[25,26] and that excess copper could be removed from the human body—in comparison to gold and silver—make it an important noble metal, which could be of paramount importance for superior biomedical applications.

Herein we report the synthesis of red fluorescent monodispersed Cu NCs in aqueous medium by using dihydrolipoic acid, in combination with biocompatible polymer poly(vinylpyrrolidone) (PVP) as a stabilizer. The fluorescence of the composite was found to be sensitive to the pH of the

Received: August 27, 2014
Accepted: December 5, 2014
Published: December 5, 2014

DOI: 10.1021/am505799q
ACS Appl. Mater. Interfaces 2015, 7, 209−222

Scheme 1. Schematic Representation of (A) Synthesis of Cu NCs Having pH-Dependent Fluorescence; (B) Synthesis of Cu NC−Hydrogel Composite by Crosslinking PVP and PVA, and (C) Cisplatin-Loaded Cu NC-Hydrogel Composite Leading to Apoptotic Cell Death as Probed by Cellular Imaging

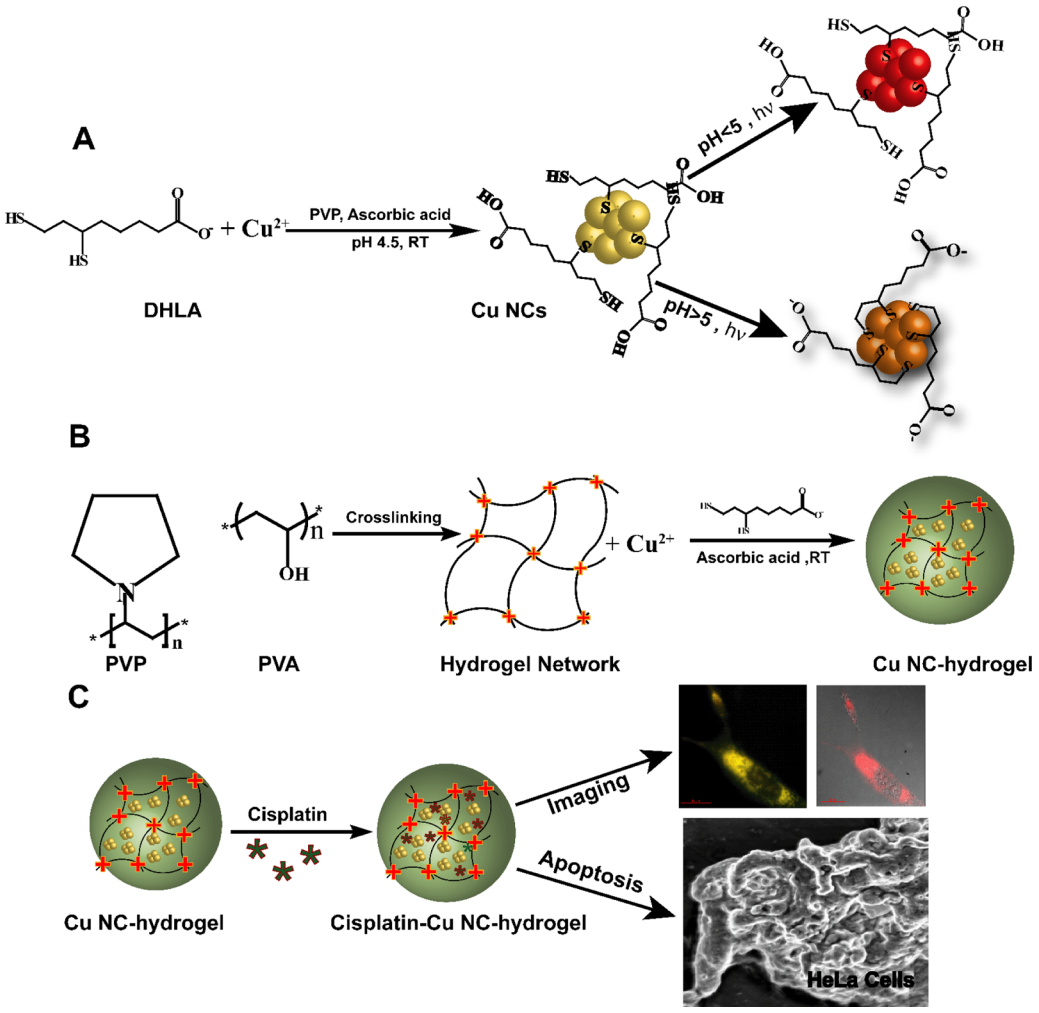

medium, and the emission could be tuned reversibly according to the pH. Also, the polymer NC composite could easily be synthesized in the form of hydrogel nanocarrier, by using poly(vinyl alcohol), PVA, as the cross-linker, which is favorable for cellular uptake.[27] The hydrogel could be then turned into a powder, which showed stable fluorescence, owing to the NCs, for more than a month. Further, the emission due to the NCs was useful for imaging mammalian cells by optical microscopy and more importantly to probe the cells by commercial flow cytometer, without having to use any other dye. Cu NC-containing hydrogel could encapsulate cisplatin (CP) for effective delivery to cancer cells, which was probed by using the emission properties of the NCs. Interestingly, it was found that Cu NCs generated reactive oxygen species in the cancer cells and hence enhanced the efficacy of CP in killing the cells, thus providing a synergy of action. The essential concept involving reaction scheme for the formation of composite of Cu NCs and PVP and its application in drug delivery as well as imaging of cells is depicted in Scheme 1.

EXPERIMENTAL SECTION

Materials. Copper chloride ($CuCl_2$), sodium hydroxide, sodium chloride, hydrochloric acid, and sodium bromide were purchased from Merck Specialties Private Limited, India. PVP, average molecular weight: 15 kDa, PVA, average molecular weight: 30 kDa, α-lipoic acid, (3-(4, 5-dimethylthiazolyl-2)-2,5-diphenyltetrazolium bromide) (MTT), and α-cyano-4-hydroxycinnamic acid were purchased from Sigma-Aldrich, U.S.A. Cisplatin was purchased from a commercial source. Milli-Q grade water (18.2 MΩ cm) was used for all experiments.

Synthesis of Copper Nanoclusters (Cu NCs). To synthesize fluorescent Cu NCs, 10.3 mg (10 mM) of α-lipoic acid was added to 5.0 mL of milli-Q water. To this insoluble mixture, 0.92 mg (5 mM) of $NaBH_4$ was added, and the mixture was stirred until the color of the medium changed from yellow to colorless, indicating the reduction of lipoic acid to dihydrolipoic acid (DHLA). Separately, 10 mg/mL of PVP was added to 3.8 mL of saturated solution of NaCl in a 15 mL culture tube, and the mixture was stirred for 2 min. To this, 0.2 mL (25 mM) of $CuCl_2$ and 3.5 mg (4 mM) of ascorbic acid were added to reduce the Cu(II) chloride to colorless Cu(I) chloride solution. This was followed by the addition of 1.0 mL (10 mM) of dihydrolipoic acid (DHLA), and the mixture was stirred for another 5 min. The final color of the mixture changed from colorless to pale yellow. The color change took place immediately after the addition of dihydrolipoic acid. The product was centrifuged at 10 000 rpm for 10 min (at 4 °C), and the precipitate was redispersed in milli-Q water and phosphate-buffered saline (PBS) (pH ≈ 7.4) for further use.

Preparation of PVP/PVA Hydrogel. Hydrogel was prepared by cross-linking of PVA and PVP (70:30 w/w) using freeze−thaw method. For this, PVP and PVA powders were mixed together containing 7.0 mL of PVA (10 mg/mL) and 3.0 mL of PVP (10 mg/

DOI: 10.1021/am505799q
ACS Appl. Mater. Interfaces 2015, 7, 209−222

mL), and the mixture was stirred while being kept at 90 °C for 24 h. Then, the mixture was kept at −20 °C for 12 h, and the frozen mixture was then allowed to melt at room temperature. The freeze−thaw step was repeated several times to induce formation of hydrogel.

Synthesis of Cu NCs in Hydrogel. Cu NCs were synthesized inside the hydrogel via in situ precipitation method. For this, 1.0 mM of $CuCl_2$ solution was added to 5.0 mL of hydrogel, then 2.6 mL of saturated solution of NaCl was added, and the mixture stirred for 10 min. After this, 4.0 mM of ascorbic acid was added, and the mixture was stirred for another 5 min. Finally, 2 mM of dihydrolipoic acid was added to it, leading to the formation of fluorescent red color inside the hydrogels. From atomic absorption spectrophotometric (AAS) analysis, it was found that 168.5 μg mL^{-1} of copper was present in the clusters synthesized with 1.0 mM of copper salt precursor.

Loading Efficiency of the Cu NC−Hydrogel Composite for Cisplatin. To determine the amount of CP loaded into the carrier Cu NC−hydrogel composite (2.0 mL, 0.5 mg of particles, corresponding to particle loading of 21.08 μg/mL) was taken in a 15 mL beaker; CP (0.1 mL of 19.6 μg/mL) was added to it, and the mixture was incubated for 24 h in the dark. The mixture was then centrifuged at 10 000 rpm for 10 min and at 4 °C. The supernatant was collected, and UV−visible spectrum was recorded for CP at 230 nm. To quantify the amount of the CP loaded in the Cu NC−hydrogel composite, the UV−visible spectrum was recorded for free CP present in the supernatant (CP_f). This was determined by measuring the absorbance at 230 nm, and the concentration so obtained was subtracted from the amount of cisplatin initially used for encapsulation (CP_i).

$$\text{loading efficiency}(\%) = \frac{CP_i - CP_f}{CP_i} \times 100$$

Analysis of Cisplatin Release from Cu Nc−Hydrogel Composite. To quantify the in vitro release of CP from Cu NC−hydrogel composite, the release profile was studied in acetate buffer (0.01 mM, pH 4.5) and PBS (0.01 mM, pH 7.4) at constant time intervals. For this, 0.5 mL of CP-loaded Cu NC−hydrogel composite was added to 1.5 mL of acetate or PBS buffer and was incubated for 48 h at 37 °C. After each time interval, that is, at 1, 3, 6, 12, 24, 36, and 48 h, the sample was centrifuged, supernatant was collected, and the amount of CP released from Cu NC−hydrogel composite was determined. The absorbance of supernatant was recorded at 230 nm, and the released CP from Cu NC−hydrogel composite in the supernatant was calculated by using the following equation.

$$\text{cumulative release}(\%) = \frac{\text{cisplatin released in the supernatant}}{\text{cisplatin loaded in the Cu NC hydrogel composite}} \times 100$$

CHARACTERIZATION

UV−visible Spectroscopic Measurements. UV−visible spectra were recoded with a Hitachi-U2900 or a PerkinElmer Lamda 25 spectrophotometer.

Fluorescence Measurements. Fluorescence spectra were recorded by using a spectrophotometer (Fluorolog −3, Horiba Jobin Edison, NY, USA). Photostability analyses of Cu NCs were carried out in the presence of continuous irradiation of ultraviolet light in the interval of time from 0.1 s to 30 min, under the excitation wavelength at 365 nm, with emission wavelength maximum being 650 nm.

Transmission Electron Microscopy (TEM). JEOL JAM 2100 TEM with maximum operating voltage of 200 kV was used for TEM measurements to analyze the size of Cu NCs. Diluted Cu NC dispersion (6.0 μL) was drop-cast on to carbon-coated copper grid and was kept for drying overnight at room temperature in the air, before making measurements.

Dynamic Light Scattering Measurements. Zeta potential and hydrodynamic diameter measurements of samples were performed by using Malvern Zeta Size Nano ZS-90 instrument at a temperature of 25 °C and using a sample viscosity of 0.8872 mPa·s.

Fourier Transform Infrared Spectroscopy. FTIR spectroscopic measurements were carried out by using PerkinElmer Spectrum One model in the range of 400−4000 cm^{-1}. For FTIR measurements, samples were prepared by drying in vacuum and then making the pellets with KBr, before recording the spectra.

Matrix-Assisted Laser Desorption Ionization Time-of−Flight mass spectrometric (MALDI-TOF-MS) Measurements. Applied Bio systems 4800 Plus MALDI TOF/TOF Analyzer was used with α-cyano-4-hydroxycinnamic acid as the matrix for MALDI-TOF-MS analysis. Mass spectra were collected in the linear negative mode with low mass. The matrix was prepared as follows. α-Cyano-4-hydroxycinnamic acid (10 mg) was dissolved in mixture of solvents of acetonitrile and trifluoroacetic acid in the ratio of 1:3, and water was used to make the volume equal to 1.0 mL. The samples were prepared by mixing Cu NCs with matrix in different ratios such as 1:1, 1:2, and 1:3; the mixtures were mixed thoroughly, and from this 0.8 μL of each sample was used for spotting.

Field-Emission Scanning Electron Microscopy (FESEM). FESEM analyses of the samples were carried out in a Carl Zeiss, SIGMA VP instrument. FESEM samples were prepared by drop-casting on a glass slide that was covered with aluminum foil and left standing overnight in the air for drying. Those samples were sputter-coated with a gold film using a sputter coater (SC 7620 "Mini", Polaron Q Sputter Coater Quorun Technologies, Newhaven, England), before analyzing under FESEM.

X-ray Photoelectron Spectroscopy (XPS). PHI 5000 VersaProbeII scanning XPS microprobe was used for X-ray photoelectron spectroscopy (XPS) measurements for Cu NCs. Samples were prepared as pellets and were introduced into the XPS prechamber under ultrahigh vacuum conditions before final measurement.

Quantum Yield Measurements of Cu NCs. Quantum yield measurement of Cu NCs was carried out by using quinine sulfate (dissolved in 0.1 M H_2SO_4) as a reference, following standard protocol.[28] The Cu NCs were used as such after synthesis. The quantum yield was calculated by using the following equation.

$$Q_{CuNC} = Q_{ref} \frac{m_{CuNC}}{m_{ref}} \frac{n_{CuNC}^2}{n_{ref}^2}$$

where $Q_{Cu\ NCs}$ and Q_{ref} are the quantum yield of Cu NCs and quinine sulfate, respectively; $m_{Cu\ NCs}$ and m_{ref} are the slopes of the plot of integrated fluorescence intensity versus absorbance of Cu NCs and quinine sulfate, respectively; and $n_{Cu\ NCs}$ and n_{ref} are the refractive indices of Cu NCs and the reference, respectively, in distilled water (assumed to be equal to that of water, that is, 1.33). The emission spectra for the samples were recorded at the excitation wavelength of 365 nm, keeping the slit width at 2 nm.

Cell Culture. HeLa cells (human cervical carcinoma) were obtained from National Centre for Cell Sciences (NCCS) Pune, India, and cultured in Dulbecco's Modified Eagle's Medium (DMEM) complemented with L-glutamine (4 mM), penicillin (50 units/mL), streptomycin (50 mg/mL)—which were purchased from sigma Aldrich—and 10% (v/v) fetal

DOI: 10.1021/am505799q
ACS Appl. Mater. Interfaces 2015, 7, 209−222

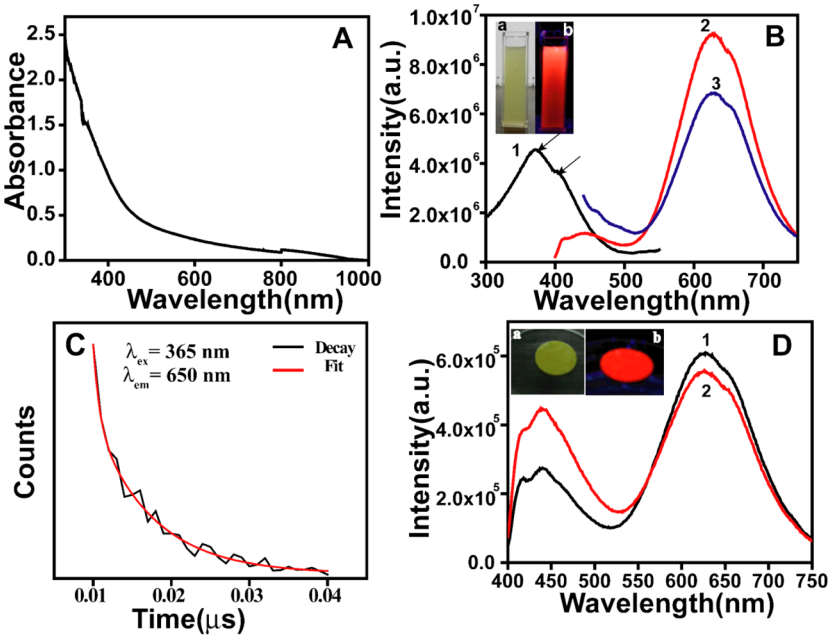

Figure 1. (A) UV−visible spectrum of as-synthesized Cu NCs formed by the reaction of Cu^{2+} with dihydrolipoic acid in the presence of PVP. (B) Excitation spectrum of Cu NCs (curve 1) with emission maximum at 650 nm. Emission spectra of Cu NCs with λ_{ex} = 365 nm (curve 2) and λ_{ex} = 405 nm (curve 3). Arrows in curve 1 show the excitation maxima at 365 and 405 nm, respectively. (inset) Photographs of dispersions of Cu NCs under (a) daylight and (b) UV light. (C) Fluorescence decay profile of Cu NCs excited at λ_{ex} = 365 nm, with emission peak being set at 650 nm. (D) Fluorescence spectrum of as-prepared Cu NCs in solid form (curve 1) and the same after one month (curve 2). (inset) Photographs of Cu NCs in solid form under (a) daylight and (b) UV light.

bovine serum (FBS, purchased from PAA Laboratories, Austria), being kept in a 5% CO_2 incubator at 37 °C.

FESEM and TEM Analysis for Untreated and Treated Cells. For TEM and FESEM analyses, HeLa cells were seeded in a 35 mm cell culture plate and nursed for 24 h. After that the CP-loaded Cu NC−hydrogel composite was added to the cells and kept for 3 h. For control sample, cells were incubated in media without the composite. After 3 h of incubation, cells were washed with PBS a number of times. Then, the cells were trypsinized, centrifuged, and fixed in glutaraldehyde solution (2%) for 10 min. The cells were then dehydrated in chilled ethanol solution and finally dispersed in absolute ethanol. For TEM sample preparation, 10 μL of the cell dispersion was drop-cast on carbon-coated copper grid and was then kept for drying in the air. For FESEM analysis, 20 μL of samples were drop-cast onto the glass slide covered with aluminum foil and was then kept for drying in the air.

Epifluorescence Microscopy. For cell imaging, 1×10^5 HeLa cells were seeded in six-well cell culture plate and grown for 24 h. HeLa cells were incubated with Cu NC−hydrogel composite or CP-loaded Cu NC−hydrogel composite for another 2 h. After 2 h of incubation, the medium was removed and the cells were washed with PBS. Finally, 1 mL of PBS was added to the plate and the cells were analyzed under epi-fluorescence microscope (Nikon ECLIPSE TS100, Tokyo) for observing the fluorescence of NCs inside the cells. For imaging, the excitation band-pass filters used were blue (340−380 nm) and green (540/25 nm) and emission band-pass filters used were green (515−555 nm) and red (655/55 nm).

Cell Viability Assay. Cell viability assay was carried out to quantify the viable cells after treatment with Cu NC−hydrogel composite and CP-loaded Cu NCs−hydrogel composite. About 1×10^4 cells/well were seeded in 96-well micro plate and were incubated in DMEM media for 24 h in the presence of 5% CO_2 at 37 °C. Then, CP-loaded Cu NC−hydrogel composite—with various concentrations (3.2−15.7 μg/mL)—was added to the cells and kept for 24 h under similar conditions. After 24 h of incubation, cell viability assay was performed which was followed by MTT assay in which tetrazolium salt, MTT [3-(4,5-dimethylthiazol-2-yl)-2,5-diphenyltetrazolium bromide] was reduced into purple colored formazan by respiring mitochondria present in the live cells. For the reaction, 7.0 μL of MTT was added to each well of the microplate and kept for 2 h in 5% CO_2 at 37 °C for the formation of formazan. After 2 h of incubation, the medium was removed and 60 μL of DMSO was added to each well for the development of purple color due to the formation of formazan, which absorbs at 550 nm. The control experiments were carried out in similar ways with various amounts of CP (1.5−8.4 μg/mL) and Cu NC−hydrogel composite (3.2−15.7 μg/mL). All the experiments were carried out in triplicate. The percentage of cell viability of control was taken as 100%. The cell viability was calculated by using the standard formula.

$$\%\text{viable cells} = \frac{(A_{550} - A_{690})\text{treated cells}}{(A_{550} - A_{690})\text{control cells}} \times 100$$

A_{550} and A_{690} are the absorbance at 550 and 690 nm corresponding to the formation of formazan and control medium, respectively.

Fluorescence-Activated Cell Sorting Analysis for Uptake of Cu NC−Hydrogel Composite. The cellular uptake of Cu NC−hydrogel composite was studied by using a flow cytometer. For this, 1×10^5 cells were seeded in 60 mm tissue culture plate for 24 h at 37 °C. Then, Cu NC−hydrogel composite (8.9 μg/mL) or CP-loaded Cu NC−hydrogel composite (8.9 μg/mL) was added to the plate and incubated for 3 h under the same condition. After incubation, the residual

DOI: 10.1021/am505799q
ACS Appl. Mater. Interfaces 2015, 7, 209−222

media were removed, and the plate was washed with PBS and trypsinized. Finally, the cells were centrifuged at 650 rcf for 5 min, and the cells were redispersed in PBS. The samples were analyzed by fluorescence-activated cell sorting (FACS) calibur (BD Biosciences), and the fluorescence of Cu NCs in the composite was recorded with the Cell Quest pro in different channels such as FL2 (band-pass filter 585/42 nm) and FL3 (low pass filter, 670 nm). For each run 15 000 cells were used.

FACS Analysis for Reactive Oxygen Species Generation. To analyze the generation of reactive oxygen species (ROS) inside the cells by Cu NC−hydrogel composite and CP-loaded Cu NC−hydrogel composite, 2′,7′-dichlorofluorecein-diacetate (DCFH-DA) staining was performed, followed by measurement using FACS calibur instrument. DCFH-DA is a nonfluorescent dye, and it diffuses into the cell through plasma membrane and is converted to DCFH by cellular esterase activity. The nonfluorescent DCFH is converted to green fluorescent 2′,7′-dichlorofluorecein (DCF) by intracellular oxidation, which absorbs at 488 nm and emits at 530 nm. For this, 2×10^5 HeLa cells were seeded in a six-well plate for 24 h. After 24 h of incubation, CP-loaded Cu NC−hydrogel composite (8.9 μg/mL) was added and kept for 3 h. After 3 h of incubation, the residual medium was removed, and the cells were washed with PBS several times. Finally, the cells were trypsinized, redispersed in 1.0 mL of fresh DMEM in which 5.0 μL of 1.0 mM of DCFH-DA was present, and incubated for 10 min at 37 °C. After incubation, the samples were analyzed for the fluorescence of DCF by flow cytometer using Cell Quest pro in fluorescence channel for 15 000 cells for each sample. The same procedure was repeated with HeLa cells treated with CP (4.5 μg/mL) and Cu NC−hydrogel composite (8.9 μg/mL). Experiments were carried out in triplicate.

RESULTS AND DISCUSSION

Red fluorescent Cu NCs were synthesized in aqueous medium at room temperature, by a simple and fast process, involving the reduction of Cu^{2+} ions by ascorbic acid and DHLA in the presence of PVP as the stabilizer. Ascorbic acid reduced Cu^{2+} to Cu^{+} ions in the presence of saturated solution of NaCl, as observed by change in the color of the medium from yellow to colorless.[29] Upon addition of DHLA the color of the solution changed from yellow to colorless accompanied by a slight precipitation. The UV−visible spectrum of the pale yellow reaction mixture, recorded after 30 min of mixing the reactants (Figure 1A), consisted of a featureless broad background and did not exhibit any peak in the region of 500−600 nm, thus excluding the formation of surface plasmon resonance (SPR) active Cu nanoparticles (NPs). The medium appeared fluorescent red under a UV lamp (Figure 1B), which indicated the formation of Cu NCs. The fluorescence spectrum of the yellow product in water exhibited two emission peaks centered at 435 and 650 nm, when excited at either 365 or 405 nm (Figure 1B). The low-energy excitation peak (at 405 nm) of the Cu NCs might be originating from the ligand-to-metal charge transfer (LMCT), whereas the high-energy excitation peak (at 365 nm) might originate from the dihydrolipoic acid ligand through intraligand as well as metal-perturbed intraligand transition.[30,31] On the other hand, the dual emission peaks of metal NCs (stabilized by the ligand) may arise either from the interband electronic transition or intraband transition.[20] However, according to Yam et al. the high-energy emission peak is due to the metal perturbed intraligand phosphorescence, whereas the low-energy emission peak may be due to LMCT.[30,31] Also, it is known that the emission properties are dependent on the size of clusters.[19] The dual emission of Cu NCs originated either from the same-sized clusters as described above or from different sizes of clusters. As our results indicate that two emissions are independent of the excitation wavelength, the emissions may be coming from the same-sized cluster. To examine whether LMCT from the triplet excited state of Cu NCs was occurring in our system, we carried out time-correlated single photon counting fluorescent experiments. A long radiative lifetime of 0.8 μs in these experiments (Figure 1C) supported that the emission had its origin in the excited triplet state of a ligand and through charge transfer to metal.[20,23,30,31] Importantly, the emission spectrum was similar to that reported in the literature for Cu NCs, thus indicating the formation of Cu NCs. That the fluorescent spectrum did not change after 20 min of formation of Cu NCs suggests that their formation was complete within a few minutes (Figure S1, Supporting Information). Interestingly, the so-prepared Cu NCs could be stored for a long time in the solid form. Centrifugation of the product resulted in the precipitate that was dried and stored in the form of a pellet, which appeared bright fluorescent red under a UV lamp. The fluorescence spectrum of the pellet with a peak at 635 nm was nearly the same as that of the product from the medium (Figure 1D). Additionally, the fluorescence spectrum of the solid recorded after one month showed almost no change, thus indicating the superior stability of the solid Cu NCs (Figure 1D, inset). Importantly, solid Cu NCs also appeared bright fluorescent red under the UV lamp. The prime challenge while working with Cu NCs is their instability under ambient conditions, due to the ease of oxidization of Cu (0) to Cu^{2+} (E_0 = 0.34 V) in comparison to Ag (E_0 = 0.80 V) or Au (E_0 = 1.50 V). Thus, by this method not only were fluorescent Cu NCs formed but also were easy to store in solid form without using any inert atmosphere. For analyzing the role of all reagents for the formation and stability of Cu NCs in aqueous medium, several control experiments were performed (Figure S2, Supporting Information). The emission results in Figure S2, Supporting Information, indicate that in the presence of PVP not only were the NCs stable but also had higher emission intensity. It is reported that PVP stabilizes NCs through weak coordination bonds.[32] The excess chloride ion present in saturated solution of NaCl helped in forming Cu(I) chloride, which is then easily reduced to Cu(0) in the presence of ascorbic acid.[29] It was also observed that Cu NCs synthesized in aqueous medium by using PVP as a stabilizer were stable as long as 3 d; the fluorescent intensity decreased quickly with time, indicating that the Cu NCs became unstable in the long run (Figure S3, Supporting Information).

Further investigation indicated that the emission spectrum (and thus the fluorescent color) of the dispersion of as-synthesized Cu NCs in water could be tuned reversibly by changing the pH of the medium. The Cu NCs synthesized at pH 4.5 emitted a red fluorescence at 650 nm (λ_{ex} = 365 nm). It is important to mention here that there was slight precipitation from the dispersion when kept at pH 4.5. This could be due to protonation of the carboxylic acid (−COOH) group and one of the thiol (−SH) groups of dihydrolipoic acid, while the second thiol group in the deprotonated state could be bonded to the NC. When the pH was increased clear solution resulted (at pH 6.5) and it remained so up to a pH of 11.0. The pH change from 4.5 to 11.0 was accompanied by an increase in the fluorescence intensity (Figure 2A), which could be attributed to

DOI: 10.1021/am505799q
ACS Appl. Mater. Interfaces 2015, 7, 209−222

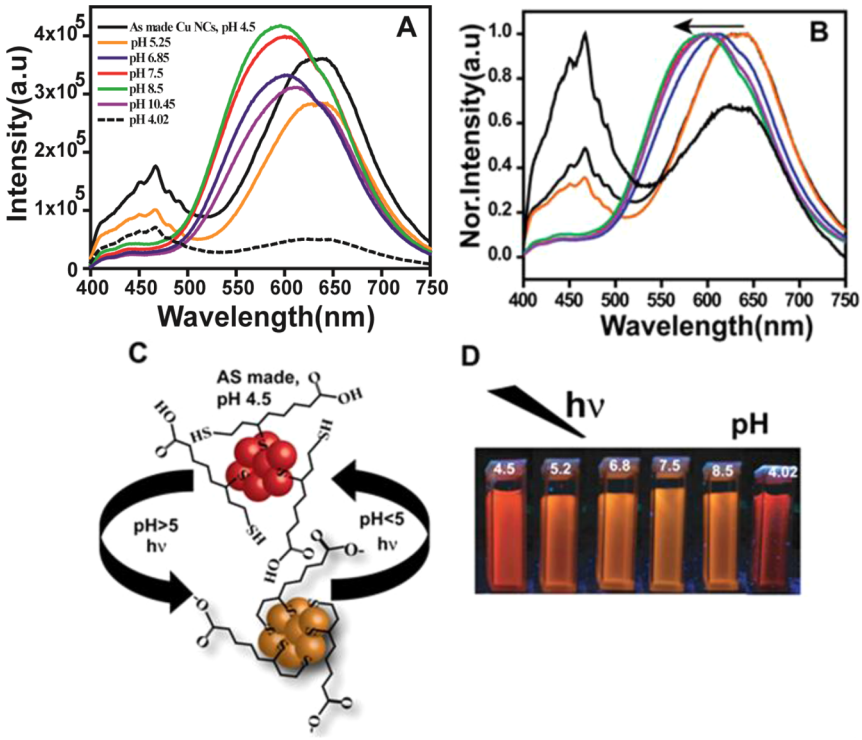

Figure 2. (A) Fluorescence spectra of as-synthesized Cu NC dispersions in the pH range of 4.5−11.0. (B) Normalized fluorescence spectra of as-synthesized Cu NCs in the pH range of 4.5−11. The arrows indicate the shift of wavelength in the pH range of 4.5−11. (C) Schematic representation of chemistry for the reversibility of fluorescence color from red to orange (and emission) by change in pH. (D) Photographs of Cu NCs under UV lamp (λ_{ex} = 365 nm) in the pH range of 4.5 to 8.5.

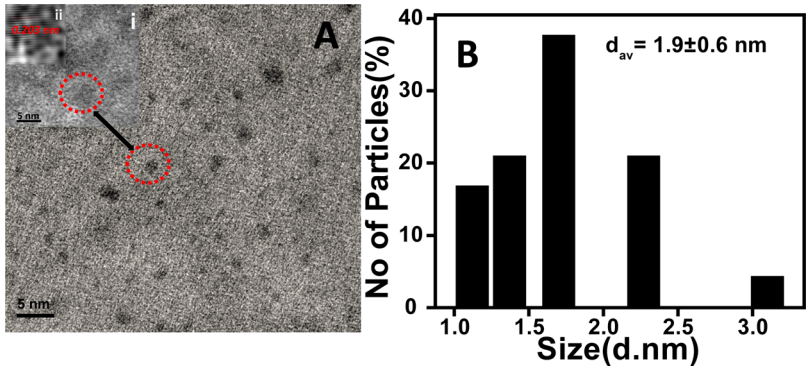

Figure 3. (A) TEM image of as-synthesized Cu NCs (with 5 nm scale bar). Inset (i) is the HRTEM images of a large Cu nanoparticle and (ii) IFFT image of the nanoparticle with lattice spacing of 0.203 nm corresponding to the (111) plane of Cu(0). (B) Particle size histogram of Cu NCs as obtained from TEM measurement (Figure 3A). The size distribution of Cu NCs was calculated from several images (from the same sample) and by considering more than 100 particles.

the deprotonation of the COOH as well as the remaining SH group of DHLA. Accompanying the increase in fluorescence intensity, the emission maximum shifted from 650 to 590 nm (at pH 6.5 and beyond, Figure 2B), while the color of the dispersion changed from fluorescent red to orange (Figure 2C, D). The change in color and emission maximum of Cu NCs depend on the surface anchoring groups of NCs. This could be attributed to the charge transfer from the ligand to metal core of NCs (Cu atoms) through Cu−S bonds.[30,31,33] Importantly, the fluorescence emission spectrum could be reversibly switched between pH 4.5 and 11.0 (Figure 2C,D).

The fluorescence quantum yield at different pH values of the medium was determined using quinine sulfate (having quantum yield of 54%) as the standard. The quantum yield was found to be 7.2% at pH 4.5, whereas it was 10.8% at pH 8.5 (Figure S4, Supporting Information). The results indicated not only the brightly emissive nature of Cu NCs but also the pH tuneability of the emission, which may be useful for practical applications.

TEM analysis of drop-cast as-synthesized sample revealed the presence of small particles with diameter 1.9 ± 0.6 nm (Figure 3). There was also the presence of agglomerated structures with diameters greater than 2 nm. Literature reports suggest enhancement of fluorescence quantum yield due to agglomeration,[22] which may well be the case herein. Further, high-resolution TEM (HRTEM) analysis did not reveal the clear lattice fringes for the smaller particles; however, for some of the bigger particles (with diameter >2 nm) fringes with lattice spacing 0.203 nm, corresponding to the (111) plane of Cu (0)

DOI: 10.1021/am505799q
ACS Appl. Mater. Interfaces 2015, 7, 209−222

(Figure 3A, inset (i) and (ii)) could be observed. It could be that some nanoscale particles with larger sizes were formed in the medium; however, their concentration was sufficiently low in the medium to give rise to any SPR band. Additionally, a single band obtained in 1.2% agarose gel electrophoresis suggested monodispersed nature of the synthesized Cu NCs (Figure S5, Supporting Information).

FTIR spectral measurement (Figure S6, Supporting Information) revealed that the characteristic peak of S−H stretch of DHLA at 2585 cm^{-1} was absent in the composite containing Cu NCs following their formation. The results indicated the possibility of stabilization of the NCs through Cu−S−R bonding.

Among the noble metals, Cu has the highest oxidation tendency owing to its lowest reduction potential, and this is an important challenge to overcome for obtaining stable NCs. In this context, it is important to determine the oxidation state of Cu in the composite. Thus, X-ray photoelectron spectroscopy (XPS) measurements were carried out to probe the oxidation state of Cu in the NCs (Figure 4). XPS spectrum indicated the

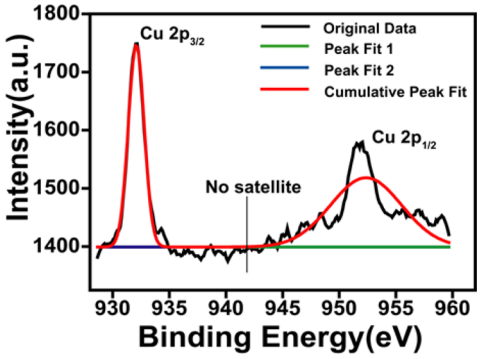

Figure 4. XPS spectrum representing the Cu 2p signal of as-prepared Cu NCs. The absence of satellite peak at 942 eV indicated the absence of Cu^{2+} in Cu NC samples.

presence of two peaks at 932.0 and 951.8 eV, which were assigned to Cu $2p_{3/2}$ and Cu $2p_{1/2}$ states of Cu(0), consistent with the literature values.[19,20] Importantly, the absence of any peak at 942.0 eV indicated the absence of Cu^{2+} in Cu NC samples. Further XPS probe of the sample indicated the presence of C, N, O, and S in the Cu NC composite sample (Figure S7, Supporting Information). It is also noteworthy that the small difference in binding energy of Cu(0) and Cu(I) (~0.1 eV) is difficult to distinguish in the XPS spectrum. Therefore, the valence state of Cu in our NCs may be 0 or +1, and possibly some of the surface Cu atoms may be partially oxidized. The binding energy of sulfur (S) 2p was found to be 163.0 eV, which indicated the possible adsorption of sulfur on the surface of Cu NCs through Cu−S bonding.[34] The result is consistent with FTIR spectrum of the NC sample (Figure S5, Supporting Information).

The atomic composition of the Cu NCs was analyzed by MALDI-TOF MS spectrometric analysis in the negative mode, using α-cyano-4- hydroxycinnamic acid as a matrix. Four prominent peaks (Figure 5) appeared at m/z 1080, 1103, 1126, and 1148, which can be attributed to $[Cu_4L_4 - 6H^+]^{6-}$, $[Cu_4L_4 - 6H^+ + Na^+]^{5-}$, $[Cu_4L_4 - 6H^+ + 2Na^+]^{4-}$ and $[Cu_4L_4 - 6H^+ + 3Na^+]^{3-}$, respectively, where L is $C_8H_{16}O_2S_2$. The results indicated the formation of monodispersed Cu NCs with molecular formula of Cu_4. In addition, MALDI-TOF MS

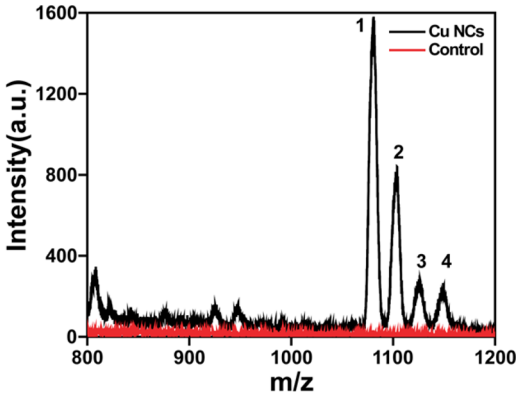

Figure 5. MALDI-TOF MS spectra of Cu NCs (in black) and control containing DHLA and PVP (in red) with the assignment of the characteristics peaks due to (1) $[Cu_4L_4 - 6H^+]^{6-}$, (2) $[Cu_4L_4 - 6H^+ + Na^+]^{5-}$, (3) $[Cu_4L_4 - 6H^+ + 2Na^+]^{4-}$ and (4) $[Cu_4L_4 - 6H^+ + 3Na]^{3-}$.

analysis of Cu NCs were carried out at different pH (i.e., 6.5, 8.5, and 10.5), which confirmed that the size of Cu NCs remained same from pH acidic to highly basic medium (Figure S8, Supporting Information). Also, the reversible nature of the observation suggests that the sizes of the emitting particles were not altered.

Furthermore, the photostability of Cu NCs revealed the importance of the NCs for bioimaging and cell labeling applications. The fluorescence intensity of Cu NCs in acidic pH remained unaltered under continuous irradiation of UV light in the time interval of 0.1 s, whereas in basic pH the intensity decreased slightly; however under both conditions the decrease was much less in comparison to organic dye rhodamine 6G (Figure S9, Supporting Information). The fluorescence intensity decrease rate (F/F_0) of Cu NCs measured at the maxima in acidic pH (pH 4.5) and basic pH (pH 8) were found to be 0.037% and 0.24%, respectively, whereas in case of rhodamine 6G, the rate was found to be 0.43%. The resistance to photobleaching and their stability in solid form make the Cu NCs strong candidates for biological applications.

Additionally, zeta potential measurements were performed at different pH of the medium to find out the surface charge of Cu NCs. The as-prepared Cu NCs stabilized by PVP was found to have zeta potential of −4.09 mV (at pH 4.5), the value changed to −15.8 mV at pH 9.0 (Table S1, Supporting Information). It is plausible that at acidic pH, the NCs were stabilized by the $-NH_3^+$ of PVP and −COOH group of DHLA, whereas in basic medium the stabilizing groups are $-NH_2$ and −COO−, thus changing the emission behavior of the NCs.

The bright fluorescence, highly photostable and small size of Cu NCs could make them ideal candidates for biological application such as cellular labeling and bioimaging. For example, their fluorescence properties could be used for tracking the drug delivery in cells, which could have competitive edge over much popularized but toxic semiconductor quantum dots. To test the feasibility of their use, Cu NCs were synthesized in PVP/PVA hydrogel, and the composite was used as a nanocarrier for drug delivery in HeLa cells. PVP and PVA are hydrophilic and biodegradable polymers approved by FDA for medical applications. These polymers have been extensively used for synthesizing hydrogels for drug delivery and other pharmaceutical applications.[35,36] Hydrogels are three-dimensional network structures with high amount of water content,

DOI: 10.1021/am505799q
ACS Appl. Mater. Interfaces 2015, 7, 209−222

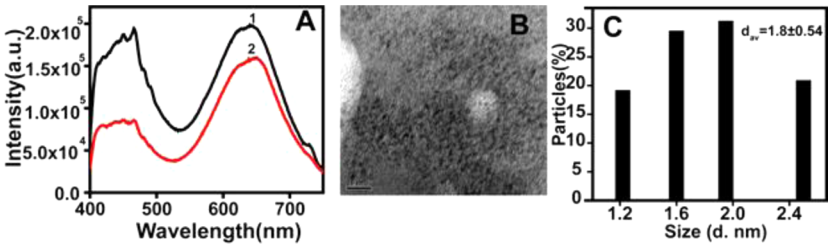

Figure 6. (A) Fluorescence spectra of Cu NCs (curve 1) and Cu NC−hydrogel composite (curve 2). (B) TEM image of Cu NCs in the hydrogel. Scale bar is 10 nm. (C) Size distribution histogram of Cu NCs in the hydrogel (as obtained from Figure 6B).

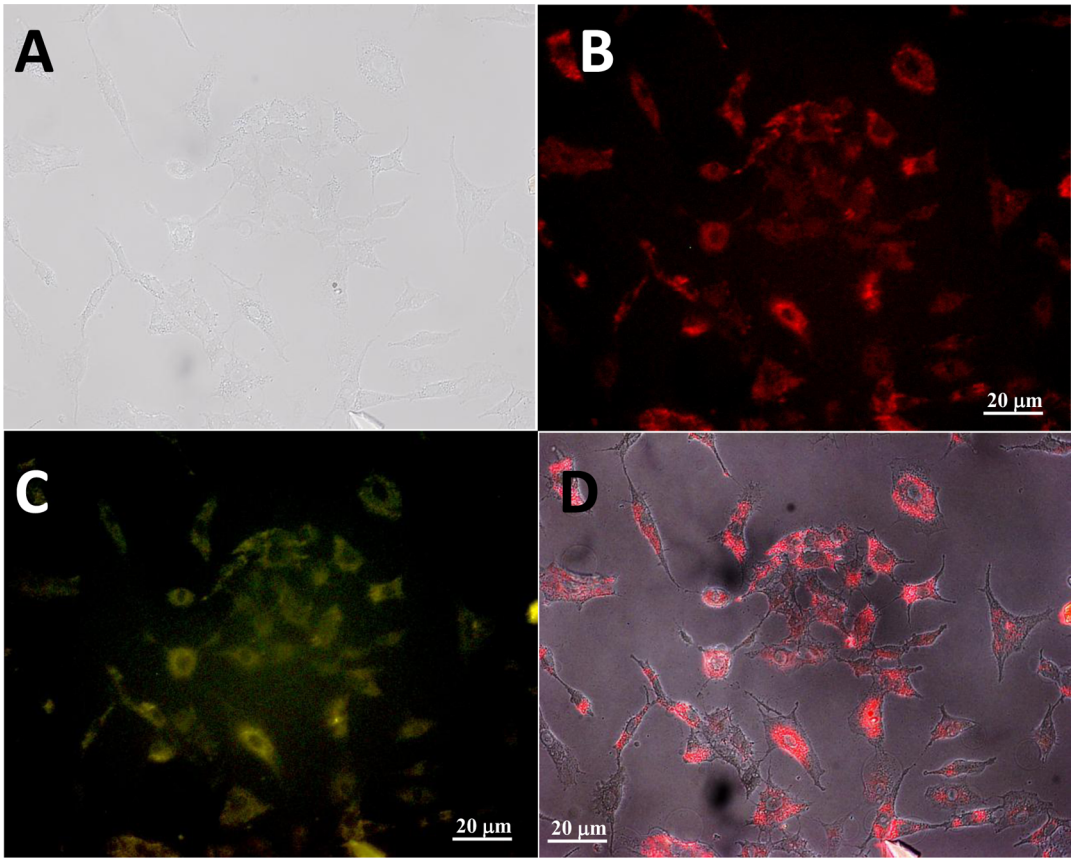

Figure 7. Epifluorescence microscopic images of HeLa cells incubated with Cu NC−hydrogel composite after 2 h. (A) Image under bright field; (B, C) fluorescence images of HeLa cells under excitation filter of blue (465−495 nm) and green (540/25 nm) with corresponding emission band-pass filters green (515−555 nm), and red (605/55 nm), respectively. (D) Microscopic merged image with bright field under same green excitation light of the same cells. Scale bar is 20 μm.

which are ideal for loading water-soluble drugs/molecules. Here, PVP/PVA hydrogel was synthesized by using a method based on freeze−thaw cycle and such formation was confirmed by TEM and FTIR analytical methods. TEM measurement indicated the spherical nature of the hydrogel particles with average diameter of 155 ± 32 nm (Figure S10A, Supporting Information). FTIR spectra of PVA, PVP, and the hydrogel are shown in Figure S10B, Supporting Information. The broad band at 3420 cm^{-1} represents the presence of hydrogen-bonded structures and thus hydrophilic nature of the hydrogel. PVA showed bands at 3429 and 1088 cm^{-1} corresponding to O−H group and crystalline structure of PVA, respectively; whereas PVP showed a sharp band at 1657 cm^{-1}, which is due to −C═O stretching vibration. The formation of the hydrogel through physical cross-linking was indicated by the shift of −C═O stretching frequency to 1643 cm^{-1}; whereas the peak due to the crystalline structure of PVA shifted to 1099 cm^{-1}, indicating the change in the structure.[37] Further, the polymer hydrogel was characterized by differential scanning calorimeter (DSC) in order to find its transition temperature. The DSC thermogram of the hydrogel showed a single glass transition temperature (Figure S11, Supporting Information) at 80 °C, which indicated the interaction between two constituent polymers.[38]

An important challenge is the synthesis of Cu NCs with intact property (as in the above) in the hydrogel. Interestingly, Cu NCs could be synthesized in hydrogels without much change of the reaction condition. The optical properties of the NCs in the hydrogel were nearly the same as those in PVP. For example, the emission spectrum of Cu NC−hydrogel composite comprised of a peak at 640 nm with an excitation maximum at 365 nm (Figure 6A). Importantly, the average size

DOI: 10.1021/am505799q
ACS Appl. Mater. Interfaces 2015, 7, 209−222

of the NCs in PVP/PVA hydrogel was found to be 1.8 ± 0.5 nm, which is close to the size of the particles generated in PVP polymer (Figure 6B, C).

The brightly fluorescent Cu NCs in the hydrogel were further used to investigate the therapeutic and imaging potential of the composite. The composite was used to probe CP delivery to cancer cells and to find the synergy of action of the two (Cu NCs and CP), if any. In addition to the optical properties for imaging application, the size of the composite particle is important for cellular uptake. The hydrodynamic diameter of hydrogel (only) probed using dynamic light scattering (DLS) measurement was found to be 220 nm; whereas the same for Cu NC−hydrogel composite was found to be 284 nm. On addition of CP to Cu NC−hydrogel composite, the size increased further. The average hydrodynamic diameter of CP-loaded Cu NC−hydrogel composite was found to be 345 nm (Figure S12, Supporting Information). The size, although appears to be on the higher side of permissible limit for in vivo applications, still it is known to be effective for drug delivery to cancer cells. It is well-established that in tumor tissues the presence of larger pores—in comparison to healthy tissues−permits enhanced permeation and retention (EPR) of larger particles. The permeability of nanoscale particles of sizes up to 400 nm has been reported. Therefore, CP-loaded Cu NC−hydrogel with higher in size could be internalized by cancer tissues.[39]

The encapsulation of CP into the Cu NC−hydrogel composite was confirmed by FTIR and fluorescence spectroscopy. The sharp N−H and Pt−N stretching bands for CP were present at 3444 and 519 cm^{-1}, respectively, along with the bands of hydrogel at 1647 cm^{-1} and 1076 cm^{-1} (Figure S13B, Supporting Information). Fluorescence spectroscopic investigation supported interaction between composite and CP. For example, when CP was added to the composite, the fluorescence intensity of Cu NCs decreased, confirming interaction between them (Figure S13A, Supporting Information). The interaction between the Cu NCs and CP inside the hydrogel was further confirmed by ^1H NMR spectroscopy (Figure S14, Supporting Information). The characteristic peaks of COOH of the ligand-stabilized Cu NCs was found at 11.8 ppm, whereas the peak vanished when the NCs interacted with CP along with the appearance of the peak at 4.137 ppm due to NH_3 group. This indicated that Cu NCs were bound to CP through carboxylic groups,[40,41] leading to loss of its luminescence. The results also indicated that CP effectively diffused through the hydrogel containing NCs. Also, interaction through NH_3 group of CP suggest the stability of the clusters and preservation of activity of the drug in the medium. The loading of CP to the composite was further supported by zeta potential measurements. The zeta potentials of Cu NC−hydrogel composite and CP-loaded Cu NC−hydrogel composite, both measured at pH 7.4, were found to be −12.5 and −10.5 mV, respectively. The change of zeta potential indicated the loading of drug into the Cu NC−hydrogel composite. Additionally, stability of the composite is also important for its practical usages. The stability of the composite was investigated by the fluorescence spectroscopy. The results, shown in Figure S15, Supporting Information, indicated that with time the composite remained reasonably stable, with 50% decrease in fluorescence intensity in 48 h, at physiological pH of 7.4.

For microscopic imaging, HeLa cells were incubated with Cu NC−hydrogel composite for 2 h in Dulbecco's Modified Eagle's Medium (DMEM). Following this, the medium was removed; cells were washed with phosphate buffer saline (PBS), and finally they were observed under fluorescence microscope. As shown in Figure 7, brightly fluorescent cells with yellow and red colors could be observed. The colors correspond to emission from Cu NCs viewed using two different filters (red and green respectively). The results indicated that the composite hydrogel could potentially be used for imaging of cells, in conjunction with the delivery of drugs.

One of the important criteria of an efficient nanocarrier is its ability to encapsulate high concentration of drug molecules in each such carrier, essentially determining the loading efficiency. The loading efficiency of CP in Cu NC−hydrogel composite was determined using UV−vis spectroscopy by following absorption at 230 nm (due to the drug). The results indicated that Cu NC−hydrogel composite could be loaded with a maximum of ∼78% of CP (with 19.6 μg/mL concentration in the solution containing 1.0 mL of Cu NC−hydrogel composite). Cisplatin is highly soluble in water. It is plausible that the apparent high efficiency could be due to the loading of the molecules on the surface as well as inside the hydrogel particle and the strong bonding between −COOH of Cu NCs (being embedded in the polymer) and CP. This could be due to the hydrophilic nature of the hydrogel with extensive presence of hydrogen bonded interpenetrating network.[42] Before checking the anticancer activity of the drug-loaded composite, in vitro release kinetics was pursued using UV−vis spectroscopy. The time-dependent cumulative release profiles are shown in Figure 8, which revealed that 75% of CP was released at pH 4.5 within 24 h, whereas 52% was released at pH 7.4 in the same time. The results indicated that the release of CP was slower at physiological pH than under acidic condition. This could be due to stronger bonding between the drug molecule and hydrogel, which could be disrupted at acidic pH than at nearly neural condition. Other parameters like hydration capacity of the hydrogel and pore sizes may also contribute to pH-dependent differential release kinetics of the drug.[43] Similarly, the release of copper from Cu NC−hydrogel composite was investigated by atomic absorption spectroscopy (AAS). The results are shown in Figure S16, Supporting Information). Briefly, it was found that after 24 h of incubation at 37 °C, ∼8.8 ppm of copper was released from 21.08 μg/mL of copper—being present in Cu NC−hydrogel composite—in acetate buffer of pH 4.5.

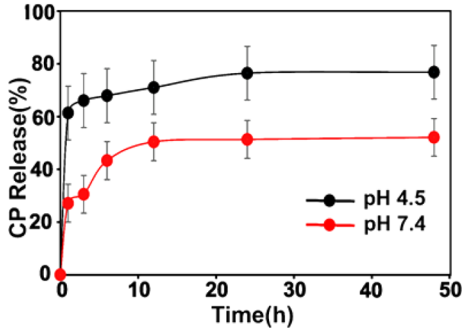

Figure 8. In vitro CP release profile (in %) from CP-loaded Cu NC−hydrogel composite over 48 h at pH 4.5 in acetate buffer (black circle) and at pH 7.4 in phosphate buffer saline (red circle). Both of the experiments were performed at 37 °C.

DOI: 10.1021/am505799q
ACS Appl. Mater. Interfaces 2015, 7, 209−222

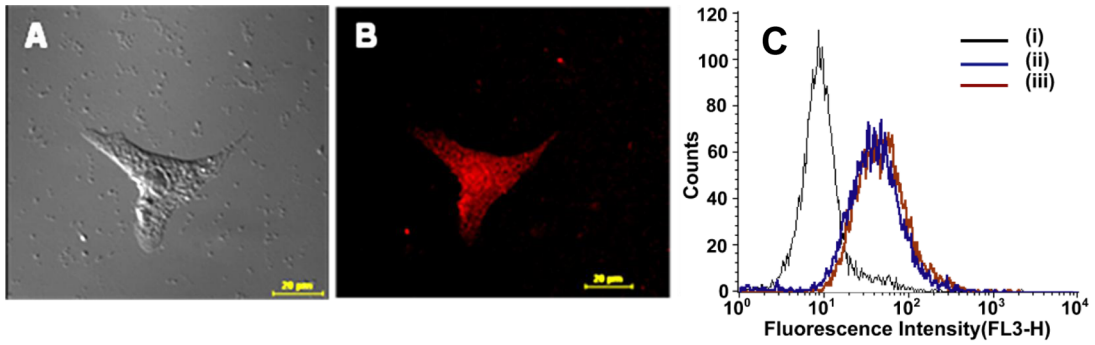

Figure 9. Confocal microscopic images of HeLa cells treated with CP-loaded Cu NC−hydrogel composite, recorded after 4 h of incubation. (A) Image under bright field and (B) fluorescence image of HeLa cells under green light. Scale bar is 20 μm. (C) FACS analysis confirming the uptake of the composite by cells as observed by shifting fluorescence intensity in FL3-H channel: (i) untreated HeLa cells, (ii) hydrogel−Cu NC (8.9 μg/mL) and (iii) CP-loaded Cu NC−hydrogel composite treated HeLa cells.

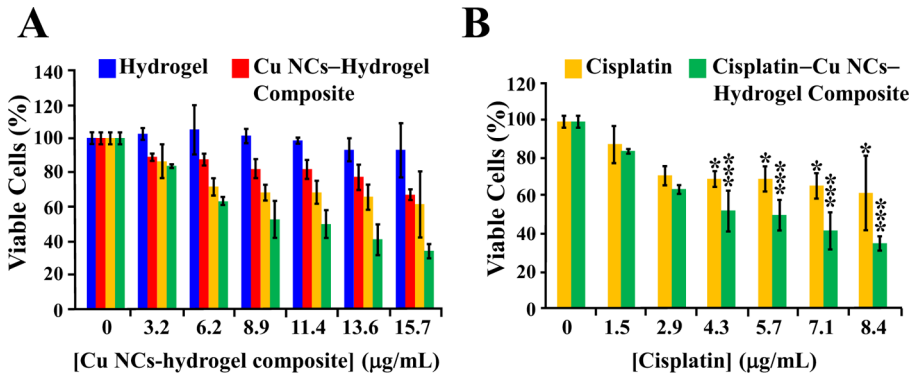

Figure 10. Viability of HeLa cells followed by MTT assay after 24 h treatment with (A) hydrogel, Cu NC−hydrogel composite and CP-loaded Cu NC−hydrogel composite with varying concentrations of the composite, free CP and CP-loaded Cu NC−hydrogel composite at varying CP concentrations; (B) CP only and CP-loaded Cu NC−hydrogel composite (shown separately from (A) for ease of comparison). Experiments were carried out in triplicate. Statistical significance was found between CP-loaded Cu NC−hydrogel composite (green line) and free CP (gray line). Statistical significance is denoted by *($p < 0.05$), **($p < 0.005$),and ***($p < 0.001$).

Finally, the utility of the drug-loaded nanocarrier is measured by its ability to work effectively against cancer cells−at least in vitro. In the current case, the uptake and release of CP-loaded Cu NC−hydrogel composite was studied in vitro following treatment with HeLa cells for 3 h in DIMEM. The cells were then analyzed by fluorescence microscopy, flow cytometry and fluorescence spectroscopy. Fluorescence microscopic images of the cells (Figure 9A,B) could easily discern the uptake of the drug loaded composite as seen by the emission due to red color under blue light excitations, respectively. In drug delivery, cellular images constitute an important indicator of the consequences of delivery. The results reported herein indicated that the NC containing drug loaded composite could be a potential candidate for real time application. Additionally, the fluorescence due to the NCs could be used to follow the cellular uptake of the loaded carrier using flow cytometry. For this, HeLa cells were independently incubated with Cu NC−hydrogel composite (8.9 μg/mL) and CP-loaded Cu NC−hydrogel composite (4.3 μg/mL of CP was loaded to 8.9 μg/mL of Cu NC−hydrogel composite) for 3 h and analyzed by fluorescence-activated cell sorting (FACS) without using any commercial dye. Cu NC−hydrogel composite and CP-loaded Cu NC−hydrogel composite showed prominent shifts in the fluorescent intensity in FL3-H (low pass/670 nm) channel in comparison to untreated cells, which correspond to red fluorescence due to the NCs (Figure 9C). The fluorescence intensity was maximum in FL3-H channel in comparison to FL1-H channel, which might be due to the Stokes shifted emission from Cu NCs with the excitation by the laser at 488 nm, which was used in the FACS Calibur instrument. Additionally, Cu NC−hydrogel composite and CP-loaded Cu NC−hydrogel composite showed almost the same shift in the FL3-H channel, which indicated the interaction between the NCs and the cells. As a result, NCs could be used for cellular tracking agent instead of commercial dyes. The cytometry results further confirmed the uptake of the free as well as drug-loaded composite by the cells. Additionally, TEM image (Figure S17, Supporting Information) of treated HeLa cells confirmed the uptake of Cu NC−hydrogel composite. A magnified image (Figure S17B,C, Supporting Information) evidenced the presence of Cu NCs inside the cells.

The significance of released drug from the CP-loaded Cu NC−hydrogel composite inside the HeLa cells was explored by cell viability assay and field-emission scanning electron microscopy (FESEM). For cell viability studies based on [3-(4,5-dimethylthiazol-2-yl)-2,5-diphenyltetrazolium bromide] (MTT) assay, cells were incubated with Cu NC−hydrogel composite, CP only, and CP-loaded Cu NC−hydrogel composite for 24 h at 37 °C. The concentration of the CP was kept in the range of 1.5−8.4 μg/mL in the composite, whereas Cu NC−hydrogel composite was used in varying concentrations from 3.2−15.7 μg/mL. Figure 10A clearly depicts that 100% of cells were viable upon incubation with hydrogel, indicating the affordable biocompatibility for the drug

DOI: 10.1021/am505799q
ACS Appl. Mater. Interfaces 2015, 7, 209−222

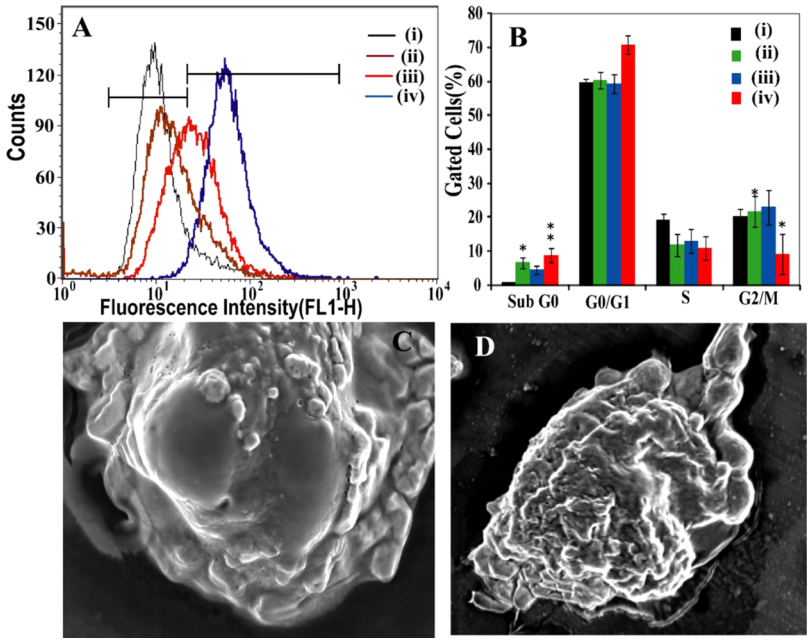

Figure 11. (A) Flow cytometric analysis of ROS production in HeLa cells: (i) untreated cells, (ii) cells treated with Cu NC−hydrogel composite, (iii) cells treated with CP only, and (iv) cells treated with CP Cu NC−hydrogel composite. (B) The effect of Cu NCs and CP in HeLa cells was analyzed by FACS in each phase of cell cycle. (i) Untreated cells, (ii) cells treated with CP only, (iii) cells treated with Cu NC−hydrogel composite, and (iv) cells treated with CP Cu NC−hydrogel composite. (C, D) FESEM images of a HeLa cells, treated with Cu NC−hydrogel composite and CP-loaded Cu NC−hydrogel composite for 24 h revealing apoptotic cell deaths. Experiments were carried out in triplicate. Statistical significance was found between free CP (green line) and CP-loaded Cu NC−hydrogel composite (red line). Statistical significance is denoted by *($p < 0.05$), **($p < 0.005$), and ***($p < 0.001$).

delivery by the hydrogel nanocomposites. Similarly, 75% of the cells were viable upon incubation with 15.7 μg/mL of the Cu NC−hydrogel composite. When the cells were treated with CP-loaded Cu NC−hydrogel composite, the cell viability decreased to 52% at 8.9 μg/mL of Cu NC−hydrogel composite, where the concentration of CP was 4.3 μg/mL. Figure 10B also shows the comparative effect of CP on cancer cells when incubated in the form of free drug molecules versus when loaded in the composite. It was found that at a concentration of 8.4 μg/mL of free CP, the cell viability was reduced to 68%, whereas at the same concentration of the drug when loaded in the composite, the viable cells were reduced to 34%. The MTT assay confirmed the potential synergistic effect of anticell proliferative Cu NC−hydrogel composite with CP on apoptosis of HeLa cells, which increased the efficacy of CP on HeLa cells. It was observed that addition of Cu NC−hydrogel composite decreased IC_{50} value of CP in HeLa cells. Figure 10B clearly shows that 70% of the cells were viable upon incubation with 4.3 μg/mL of CP only for 24 h. Addition of 8.9 μg/mL composite with 4.3 μg/mL of the CP resulted an increase in the cell death by 18%. This indicated that Cu NC−hydrogel composite could enhance the drug efficacy of the composite and can decrease the IC_{50} value of CP. The IC_{50} value of CP when loaded in the hydrogel was calculated to be 5.5 μg/mL. On the other hand, at 8.4 μg/mL of free CP cell viability was reduced to 68% only. The significant decrease of cell viability in the presence of drug-loaded carrier as opposed to free drug molecule evidenced the importance of suitable carrier for increasing the therapeutic efficacy. The result demonstrated that the combination of Cu NC−hydrogel composite and CP can be used as a potential applicant for designing new chemotherapeutic agent.

Biological utility of composites depends on the size, shape, chemical composition, solubility, and surface structures of the NPs. Metal NPs can induce oxidative stress, due to the reactive oxygen species (ROS) generation, governed by the pro-oxidant functional groups present on the surface of NPs as well as owing to the redox properties of transition metal NPs. It has been reported that Cu NPs could generate ROS in so-treated cells.[44] However, the size of the copper particles is the key determinant of toxicity. In case of NCs, the particle size is <2 nm. This shrinkage in size increases the surface-to-volume ratio and alters the electronic and chemical properties. This might create specific surface groups, which can function as reactive sites, with electron donor/acceptor properties that interact with molecular O_2 to form $O_2^{-\bullet}$. Apart from surface properties of NCs, copper can induce oxidative stress via Fenton-type reactions, where Cu ion reacts with H_2O_2 to yield $OH^{\bullet}$ and $O_2^{-\bullet}$.[45] It is also plausible that Cu^+ species present on the surface of the NC induces oxidative stress. Importantly, the rate of copper fraction release is higher when the NP is smaller in size.[46] ROS generation by Cu NC−hydrogel composite makes it not only an interesting candidate for induction of apoptosis but also provides an important potential for synergistic activity in the presence of a second drug. Interestingly, oxidative stress is associated with apoptotic cell death, which is caused by any chemotherapeutic agent.[47] Thus, flow cytometric studies of the HeLa cells treated with loaded and unloaded composite indicated induction of oxidative stress by the Cu NCs present in the composite. From Figure 11A, it is evident that the Cu NC encapsulated hydrogel generated ROS. Thus, while the cells themselves had the lowest emission intensity (FL1-H), the Cu NC−hydrogel composite-treated cells showed higher emission, which was lower than that due to the only CP-treated cells. However, CP containing composite induced

DOI: 10.1021/am505799q
ACS Appl. Mater. Interfaces 2015, 7, 209−222

highest emission intensity indicating the synergy of action of Cu NCs and CP. The percentage of ROS generation by hydrogel−Cu NC composite and CP-loaded hydrogel−Cu NC composite are shown in Figure S18 in the Supporting Information, as compared to the untreated HeLa cells and CP only. It was found that more than 20% of ROS were generated by Cu NC−hydrogel composite in comparison to untreated HeLa cells.

To pursue the synergistic effect of Cu NC−hydrogel composite and CP, we have performed cell cycle analysis by propidium iodide (PI) staining to confirm the apoptotic mode of cell death due to the oxidative stress induced by Cu NC−hydrogel composite and CP-loaded Cu NC−hydrogel composite treated cells. The flow cytometric analysis showed that the populations of cells in different stages of cell cycle such as G0/G1, S and G2/M were affected following the treatment with Cu NC−hydrogel composite and CP-loaded Cu NC−hydrogel composite in contrast to the control cells (Figure 11B). The increased percentage of population of sub G0/G1 phase of Cu NC−hydrogel composite treated cells (4.72%) and CP-loaded Cu NC−hydrogel composite treated cells (8.96%) provided primary evidence for the apoptotic mode of cell death. The cell cycle analysis for control cells and CP only, Cu NC−hydrogel composite and CP-loaded Cu NC−hydrogel composite are shown in Figure S19, Supporting Information. Further, FESEM analysis were performed on the cells treated with Cu NC−hydrogel composite and CP-loaded composite to follow the typical morphological changes of the cells following the treatment with drugs. For this, cells were incubated with Cu NC−hydrogel composite and CP-loaded Cu NC−hydrogel composite for 24 h, which was followed by imaging using FESEM (Figure 11C,D). Generally, CP binds with the guanine bases of DNA leading to cross-linking of DNA, which interferes with mitotic cell division and results in apoptotic cell death.[48] The morphological changes of the treated cells (Figure 11C,D) revealed apoptotic cell death caused by Cu NCs only and Cu NCs and CP combined, being present in the composite. FESEM analysis was also carried out for control HeLa cells where no sign of apoptosis was observed (Figure S20, Supporting Information), which was in good agreement with the cell viability assay. Further, apoptosis mode of the cell death was confirmed by the Caspase 3 assay in HeLa cells. The apoptotic cell death is primarily governed by the Caspase 3, which is a cysteine-aspartic acid protease.[49] As is evident from the caspase 3 assay results (Figure S21, Supporting Information) about 97.7% control HeLa cells were found to be nonapoptotic corresponding to M1 in the histogram of Figure S21A, Supporting Information, while 10.1% cells show apoptosis corresponding to M2 in the histogram (Figure S21C, Supporting Information), when treated with only Cu NC−hydrogel composite. Similarly, when the cells were treated with only CP, 30.9% cells had shown apoptosis whereas 38.9% cells had shown apoptosis after the treatment with CP-loaded Cu NC−hydrogel composite (Figure S21B, D, Supporting Information). The overall results indicated that Cu NC encapsulated CP-loaded hydrogel composite was more effective for apoptotic mode of cell death, which also confirmed the synergistic effect of Cu NCs and CP present in the composite. Additionally, synergy of action of CP and Cu NCs was further quantified by the combination index (CI).[50,51] The CI was determined by dose−effect profile of the drugs. The extent of interaction between the drugs was evaluated from the CI plot and such a plot gives the quantitative information about the interactions with the values of CI >1, CI <1, and CI = 0, indicating the antagonism, synergism and additivity, respectively. From Table S3 of Supporting Information, it is clear that synergistic effect was present at two cell viable points, namely, at IC_{20} and IC_{40}, in comparison to free CP and hydrogel−Cu NC composite.

CONCLUSION

In summary, we have reported the synthesis of stable and brightly fluorescent Cu NCs using a one-step process in aqueous medium. The NCs could be stabilized in the solid form, where they retained their fluorescence for more than a month. The emission property of the NCs in the aqueous medium could be tuned with pH of the medium. This is the first time that the pH tuneability of Cu NC emission is being reported. These Cu NCs, when embedded into PVP, could easily be converted to hydrogel and be used further to deliver anticancer drug CP to HeLa cells, with enhanced efficiency of killing the cells. The synergy of action of ROS generation due to Cu NCs and anticancer drug action of CP makes the composite valuable for practical application. In addition, optical imaging of the uptake of stable red fluorescent Cu NCs may find use in theranostic applications, owing to their high luminescence.

ASSOCIATED CONTENT

Supporting Information

Additional emission spectra, FTIR spectra, XPS analysis results, photostability, fluorescence decay results, zeta potential table, TEM and FESEM images, DLS measurement, NMR data, DSC thermogram results are included. This material is available free of charge via the Internet at http://pubs.acs.org.

AUTHOR INFORMATION

Corresponding Authors

*E-mail: arun@iitg.ernet.in. (A.C.)
*E-mail: anumita@iitg.ernet.in. (A.P.)

Notes

The authors declare no competing financial interest.

ACKNOWLEDGMENTS

We acknowledge the Department of Electronics and Information Technology (No. 5(9)/2012-NANO) and Department of Biotechnology (BT/49/NE/TBP/2010), Government of India, for financial support. We also thank D. Barpuzary and A. K. Sahoo for help. The authors thank Central Instrument Facilty, IIT Guwahati, for TEM and FESEM analyses.

REFERENCES

(1) Shiang, Y.-C.; Huang, C.-C.; Chang, H.-T. Gold Nanodot-based Luminescent Sensor for the Detection of Hydrogen Peroxide and Glucose. *Chem. Commun.* **2009**, 3437−3439.
(2) Wei, H.; Wang, Z.; Yang, L.; Tian, S.; Hou, H.; Lu, Y. Lysozyme-Stabilized Gold Fluorescent Cluster: Synthesis and Application as Hg^{2+} Sensor. *Analyst* **2010**, *135*, 1406−1410.
(3) Liu, B. Y.; Ai, K.; Cheng, X.; Huo, L.; Lu, L. Gold-Nanocluster-Based Fluorescent Sensors for Highly Sensitive and Selective Detection of Cyanide in Water. *Adv. Funct. Mater.* **2010**, *20*, 951−956.
(4) Wu, X.; He, X.; Wang, K.; Xie, C.; Zhou, B.; Qing, Z. Ultra Small Near-Infrared Gold Nanoclusters for Tumor Fluorescence Imaging in Vivo. *Nanoscale* **2010**, *2*, 2244−2249.
(5) Lin, C.-A. J.; Yang, T.-Y.; Lee, C.-H.; Huang, S. H.; Sperling, R. A.; Zanella, M.; Li, J. K.; Shen, J.-L.; Wang, H.-H.; Yeh, H.-I.; Parak, W.

DOI: 10.1021/am505799q
ACS Appl. Mater. Interfaces 2015, 7, 209−222

J.; Chang, W. H. Synthesis, Characterization, and Bioconjugation of Fluorescent Gold Nanoclusters Towards Biological Labeling Applications. *ACS Nano* **2009**, *3*, 395−401.
(6) Yu, J.; Choi, S.; Dickson, R. M. Shuttle-Based Fluorogenic Silver-Cluster Biolabels. *Angew. Chem., Int. Ed.* **2009**, *48*, 318−320.
(7) Tanaka, S.-I.; Miyazaki, J.; Tiwari, D. K.; Jin, T.; Inouye, Y. Fluorescent Platinum Nanoclusters: Synthesis, Purification, Characterization, and Application to Bioimaging. *Angew. Chem., Int. Ed.* **2011**, *50*, 431−435.
(8) Kauffman, D. R.; Alfonso, D.; Matranga, C.; Qian, H.; Jin, R. Experimental and Computational Investigation of Au_{25} Clusters and CO_2: A Unique Interaction and Enhanced Electrocatalytic Activity. *J. Am. Chem. Soc.* **2012**, *134*, 10237−10243.
(9) Chen, W.; Chen, S. Oxygen Electroreduction Catalyzed by Gold Nanoclusters: Strong Core Size Effects. *Angew. Chem., Int. Ed.* **2009**, *48*, 4386−4389.
(10) Zhu, Y.; Qian, H.; Drake, B. A.; Jin, R. Atomically Precise $Au_{25}(SR)_{18}$ Nanoparticles as Catalysts for the Selective Hydrogenation of α,β-Unsaturated Ketones and Aldehydes. *Angew. Chem., Int. Ed.* **2010**, *49*, 1295−1298.
(11) Sahoo, A. K.; Banerjee, S.; Ghosh, S. S.; Chattopadhyay, A. Simultaneous RGB Emitting Au Nanoclusters in Chitosan Nanoparticles for Anticancer Gene Theranostics. *ACS Appl. Mater. Interfaces* **2014**, *6*, 712−724.
(12) Shen, Z.; Duan, H.; Frey, H. Water-Soluble Fluorescent Ag Nanoclusters Obtained From Multiarm Star Poly(acrylic acid) as a "Molecular Hydrogel" Templates. *Adv. Mater.* **2007**, *19*, 349−352.
(13) Petty, J. T.; Zheng, J.; Hud, N. V.; Dickson, R. M. DNA-Templated Ag Nanocluster Formation. *J. Am. Chem. Soc.* **2004**, *126*, 5207−5212.
(14) Richards, C. I.; Choi, S.; Hsiang, J.-C.; Antoku, Y.; Vosch, T.; Bongiorno, A.; Tzeng, Y.-L.; Dickson, R. M. Oligonucleotide-Stabilized Ag Nanocluster Fluorophores. *J. Am. Chem. Soc.* **2008**, *130*, 5038−5039.
(15) Xie, J.; Zheng, Y.; Ying, J. Y. Protein-Directed Synthesis of Highly Fluorescent Gold Nanoclusters. *J. Am. Chem. Soc.* **2009**, *131*, 888−889.
(16) Liu, C.-L.; Wu, H.-T.; Hsiao, Y.-H.; Lai, C.-W.; Shih, C.-W.; Peng, Y.-K.; Tang, K.-C.; Chang, H.-W.; Chien, Y.-C.; Hsiao, J.-K.; Cheng, J.-T.; Chou, P.-T. Insulin-Directed Synthesis of Fluorescent Gold Nanoclusters: Preservation of Insulin Bioactivity and Versatility in Cell Imaging. *Angew. Chem., Int. Ed.* **2011**, *50*, 7056−7060.
(17) Kawasaki, H.; Hamaguchi, K.; Osaka, I.; Arakawa, R. pH-Dependent Synthesis of Pepsin-Mediated Gold Nanoclusters with Blue Green and Red Fluorescent Emission. *Adv. Funct. Mater.* **2011**, *21*, 3508−3515.
(18) Martin, M. N.; Li, D.; Dass, A.; Eah, S.-K. Ultrafast, 2 min Synthesis of Monolayer-Protected Gold Nanoclusters (d < 2 nm). *Nanoscale* **2012**, *4*, 4091−4094.
(19) Ghosh, R.; Sahoo, A. K.; Ghosh, S. S.; Paul, A.; Chattopadhyay, A. Blue-Emitting Copper Nanoclusters Synthesized in the Presence of Lysozyme as Candidates for Cell Labeling. *ACS Appl. Mater. Interfaces* **2014**, *6*, 3822−3828.
(20) Wei, W.; Lu, Y.; Chen, W.; Chen, S. One-Pot Synthesis, Photoluminescence, and Electrocatalytic Properties of Subnanometer-Sized Copper Clusters. *J. Am. Chem. Soc.* **2011**, *133*, 2060−2063.
(21) Jia, X.; Yang, X.; Li, J.; Lia, D.; Wang, E. Stable Cu Nanoclusters: From an Aggregation Induce Emission mechanism to Biosensing and Catalytic Applications. *Chem. Commun.* **2014**, *50*, 237−239.
(22) Jia, X.; Li, Li.; Wang, E. Cu Nanoclusters with Aggregation Induced Emission Enhancement. *Small* **2013**, *9*, 3873−3879.
(23) Jia, X.; Li, J.; Han, L.; Ren, J.; Yang, X.; Wang, E. DNA-Hosted Copper Nanoclusters for Fluorescent Identification of Single Nucleotide Polymorphisms. *ACS Nano* **2012**, *6*, 3311−3317.
(24) Wang, C.; Wang, C.; Xu, L.; Cheng, H.; Lin, Q.; Zhang, C. Protein-Directed Synthesis of pH-responsive Red Fluorescent Copper Nanoclusters and Their Applications in Cellular Imaging and Catalysis. *Nanoscale* **2014**, *6*, 1775−1781.
(25) Gaggelli, E.; Kozlowski, H.; Valensin, D.; Valensin, G. Copper Homeostasis and Neurodegenerative Disorders (Alzheimer's, Prion, and Parkinson's Diseases and Amyotrophic Lateral Sclerosis). *Chem. Rev.* **2006**, *106*, 1995−2044.
(26) Cater, M. A.; Fontaine, S. L.; Shield, K.; Deal, Y.; Mercer, J. F. ATP7B Mediates Vesicular Sequestration of Copper: Insight Into Biliary Copper Excretion. *Gastroenterology* **2006**, *130*, 493−506.
(27) Banerjee, S.; Sahoo, A. K.; Chattopadhyay, A.; Ghosh, S. S. Hydrogel Nanocarrier Encapsulated Recombinant IκBα as a Novel Anticancer Protein Therapeutics. *RSC Adv.* **2013**, *3*, 14123−14131.
(28) Lakowicz, J. R. *Principles of Fluorescence Spectroscopy,* 2nd ed.; Kluwer Academic/Plenum Publishers: New York, 1999.
(29) Xiong, J.; Wang, Y.; Xue, Q.; Wu, X. Synthesis of Highly stable dispersions of nanosized Copper particles using L-ascorbic acid. *Green Chem.* **2011**, *13*, 900−904.
(30) Yam, V. W.-W.; Cheng, E. C.-C.; Zhou, Z.-Y. A Highly Soluble Luminescent Decanuclear Gold (I) Complex with a Propeller- Shaped Structure. *Angew. Chem., Int. Ed.* **2000**, *39*, 1683−1685.
(31) Yam, V. W.-W.; Cheng, E. C.-C.; Cheung, K.-K. A Novel High-Nuclearity Luminescent Gold (I)−Sulfido Complex. *Angew. Chem., Int. Ed.* **1999**, *38*, 197−199.
(32) Mathew, A.; Sajanlal, P. R.; Pradeep, T. A Fifteen Atom Silver Cluster Confined in Bovine Serum Albumin. *J. Mater. Chem.* **2011**, *21*, 11205−11212.
(33) Wu, Z.; Jin, R. On the ligand's Role in the Fluorescence of Gold Nanoclusters. *Nano Lett.* **2010**, *10*, 2568−2573.
(34) Bensebaa, F.; Ellis, T. H.; Kruus, E.; Voicu, R.; Zhou, Y. Characterization of Self-Assembled Bilayers: Silver−Alkanethiolates. *Langmuir* **1998**, *14*, 6579−6587.
(35) Peppas, B. N. A.; Hilt, J. Z.; Khademhosseini, A.; Robert Langer, R. Hydrogels in Biology and Medicine: From Molecular Principles to Bionanotechnology. *Adv. Mater.* **2006**, *18*, 1345−1360.
(36) Bharali, D. J.; Sahoo1, S. K.; Mozumdar, S.; Maitra, A. Cross-linked Polyvinylpyrrolidone Nanoparticles:A Potential Carrier for Hydrophilic Drugs. *J. Colloid Interface Sci.* **2003**, *258*, 415−423.
(37) Gong, M.; Zhang, L.; Zuo, Y.; Zou, Q.; Wang, Y.; Wang, L.; Li, Y. Investigation on the Interpenetrating Polymer Networks (IPNs) of Polyvinyl Alcohol and Poly(N-vinyl pyrrolidone) Hydrogel and Its In Vitro Bioassessment. *J. Appl. Polym. Sci.* **2011**, DOI: 10.1002/app.
(38) Razzak, M. T.; Zainuddin; Erizal; Dewi, S. P.; Lely, H.; Taty, E.; Sukirno. The Characterization of Dressing Component Materials and radiation formation of PVA-PVP Hydrogel. *Radiat. Phys. Chem.* **1999**, *55*, 153−165.
(39) Yuan, F.; Dellian, M.; Fukumura, D.; Leunig, M.; Berk, D. A.; Torchilin, V. P.; Jain, R. K. Vascular Permiability in a Human Tumor Xenograft: Molecular size Dependence and Cutoff Size. *Cancer Res.* **1995**, *55*, 3752−3756.
(40) Xu, C. J.; Wang, B. D.; Sun, S. H. Dumbbell-like Au−Fe_3O_4 Nanoparticles for Target-Specific Platin Delivery. *J. Am. Chem. Soc.* **2009**, *131*, 4216−4217.
(41) Haxtona, K. J.; Burt, H. M. Hyperbranched Polymers for Controlled Release of Cisplatin. *Dalton Trans.* **2008**, 5872−5875.
(42) Chen, J.-P.; Leu, Y.-L.; Fang, C.-L.; Chen, C.-H.; Fang, J.-Y. Thermosensitive Hydrogels Composed of Hyaluronic Acid and Gelatin as Carriers for the Intravesical Administration of Cisplatin. *J. Pharm. Sci.* **2011**, *100*, 655−666.
(43) Hamidi, M.; Azadi, A.; Rafiei, P. Hydrogel Nanoparticles in Drug Delivery. *Adv. Drug Delivery Rev.* **2008**, *60*, 1638−1649.
(44) Jose, G. P.; Santra, S.; Mandal, S. K.; Sengupta, T. K. Singlet oxygen mediated DNA degradation by Copper Nanoparticles: Potential towards Cytotoxic effect on Cancer Cells. *J. Nanobiotechnol.* **2011**, *9*, 1−8.
(45) Nel, A.; Xia, T.; Mädler, L.; Li, N. Toxic Potential of Materials at the Nanolevel. *Science* **2006**, *311*, 622−627.
(46) Midander, K.; Cronholm, P.; Karlsson, H. L.; Elihn, K.; Möller, L.; Leygraf, C.; Wallinder, I. O. Surface Characteristics, Copper Release, and Toxicity of Nano- and Micrometer-Sized Copper and Copper(II) Oxide Particles: A Cross-Disciplinary Study. *Small* **2009**, *5*, 389−399.

DOI: 10.1021/am505799q
ACS Appl. Mater. Interfaces 2015, 7, 209−222

(47) Peng, K.-W.; Wang, H.; Qin, Z.; Wijewickrama, G. T.; Lu, M.; Wang, Z.; Bolton, J. L.; Thatcher, G. J. Selective Estrogen Receptor Modulator Delivery of Quinone Warheads to DNA Triggering Apoptosis in Breast Cancer Cells. *ACS Chem. Biol.* **2009**, *4*, 1039−1049.
(48) Guo, S.; Wang, Y.; Miao, L.; Xu, Z.; Lin, C. M.; Zhang, Y.; Huang, L. Lipid-Coated Cisplatin Nanoparticles Induce Neighboring Effect and Exhibit Enhanced Anticancer Efficacy. *ACS Nano* **2013**, *7*, 9896−9904.
(49) Sanpui, P.; Chattopadhyay, A.; Ghosh, S. S. Induction of Apoptosis in Cancer Cells at Low Silver Nanoparticle Concentrations using Chitosan Nanocarrier. *ACS Appl. Mater. Interfaces* **2011**, *3*, 218−228.
(50) Zhao, L.; Wientjes, M. G.; Au, J. L.-S. Evaluation of Combination Chemotherapy: Integration of Nonlinear Regression, Curve Shift, Isobologram, and Combination Index Analyses. *Clin. Cancer Res.* **2004**, *10*, 7994−8004.
(51) Chou, T.-C. Drug Combination Studies and Their Synergy Quantification Using the Chou-Talalay Method. *Cancer Res.* **2010**, *70*, 440−446.

DOI: 10.1021/am505799q
ACS Appl. Mater. Interfaces 2015, 7, 209−222